



HAL
open science

Monte Carlo simulations of electron interactions with the DNA molecule: A complete set of physics models for Geant4-DNA simulation toolkit

Sara Zein, Marie-Claude Bordage, Hoang Ngoc Tran, Giovanni Macetti, Alessandro Genoni, Claude Dal Cappello, Sébastien Incerti

► To cite this version:

Sara Zein, Marie-Claude Bordage, Hoang Ngoc Tran, Giovanni Macetti, Alessandro Genoni, et al.. Monte Carlo simulations of electron interactions with the DNA molecule: A complete set of physics models for Geant4-DNA simulation toolkit. Nuclear Instruments and Methods in Physics Research Section B: Beam Interactions with Materials and Atoms, 2023, 542, pp.51-60. 10.1016/j.nimb.2023.06.004 . hal-04131796

HAL Id: hal-04131796

<https://hal.science/hal-04131796>

Submitted on 26 Jun 2023

HAL is a multi-disciplinary open access archive for the deposit and dissemination of scientific research documents, whether they are published or not. The documents may come from teaching and research institutions in France or abroad, or from public or private research centers.

L'archive ouverte pluridisciplinaire **HAL**, est destinée au dépôt et à la diffusion de documents scientifiques de niveau recherche, publiés ou non, émanant des établissements d'enseignement et de recherche français ou étrangers, des laboratoires publics ou privés.

1 Monte Carlo simulations of electron interactions with the
2 DNA molecule: A complete set of physics models for Geant4-
3 DNA simulation toolkit
4
5

6 Sara A. Zein^{1*}, Marie-Claude Bordage^{2*}, Hoang Ngoc Tran¹, Giovanni Macetti³, Alessandro
7 Genoni³, Claude Dal Cappello³, Sébastien Incerti¹
8
9

10 ¹Univ. Bordeaux, CNRS, LP2I Bordeaux, UMR 5797, F-33170 Gradignan, France

11 ² Université Paul Sabatier, UMR1037 CRCT, INSERM, F-31037 Toulouse, France

12 ³ Université de Lorraine & CNRS, Laboratoire LPCT (UMR 7019), 1 Boulevard Arago,
13 57078 Metz, France

14 *Both authors contributed equally
15

16 Corresponding Author:

17 Sara A. Zein

18 Laboratoire de Physique de Deux Infinis de Bordeaux

19 19 chemin du Solarium

20 33175 Gradignan, France

21 Telephone: +33 5 57 12 08 89

22 Email: zein@lp2ib.in2p3.fr
23

24 Email addresses

25 zein@lp2ib.in2p3.fr

26 marie-claude.bordage@inserm.fr

27 tran@lp2ib.in2p3.fr

28 giovanni.macetti@univ-lorraine.fr

29 alessandro.Genoni@univ-lorraine.fr

30 claude.dal-cappello@univ-lorraine.fr

31 incerti@lp2ib.in2p3.fr
32

33 Abstract
34

35 In this study we are introducing an update of the Geant4-DNA physics constructor “option 6”
36 including electron interactions with all constituents of the DNA molecule in addition to those
37 already publicly available for liquid water. The new implementation is based on the interaction
38 cross sections of electrons with the four DNA nucleobases, deoxyribose and phosphoric acid
39 for elastic scattering, electronic excitation and ionisation in the 11 eV – 1 MeV energy range.
40 An additional sampling method to estimate the transferred secondary electron energy produced
41 by ionisation is also introduced and can be optionally activated instead of the classical
42 interpolation method based on the differential cross section tables, thus eliminating the need to
43 upload large data files. The implementation in Geant4-DNA was verified by calculating range
44 and electronic stopping power in the various materials. Good agreement is observed with the
45 data available in the literature, and calculations with the interpolation method and the sampling
46 method showed less than 4% difference. No differences were observed in terms of
47 computational cost.
48

49
50
51
52
53
54
55
56
57
58
59
60
61
62
63
64
65
66
67
68
69
70
71
72
73
74
75
76
77
78
79
80
81
82
83
84
85
86
87
88
89
90
91
92
93
94
95
96
97

Keywords: Geant4-DNA, DNA material, Monte Carlo, Electron cross sections, sampling method, Stopping power, Range.

Highlights:

- Electron interactions in DNA material
- Geant4-DNA electron transport in DNA
- Electron stopping power in DNA
- Electron range in DNA
- Ionisation sampling method

I. Introduction:

In studies of radiotherapy and radiobiology, radio-induced damage to the DNA molecule is of upmost interest since it directly affects the mortality of cells and the integrity of their replication, function and genetic expression [1]. Therefore, DNA is considered the most radio-sensitive target of the cell and radiation interaction with the backbone of the DNA (with deoxyribose sugar and phosphate group as its main components) is essential to estimate the DNA fragmentation, mostly identified by DNA strand breaks that are damages difficult to repair. In addition, damages and alterations of the nucleobases result in mutations and irregular gene expressions [2]. Upon impact, ionising radiation induces DNA damages by physical effects, through the direct ionisation and excitation of the molecule itself or, indirectly, through the creation of reactive oxygen species in the cellular medium that attack the DNA molecule. In radiobiology applications, medical physics and radioprotection, Monte Carlo simulations have been used to estimate such effects and considerable efforts have been made in the development of track structure codes able to model the radiation interaction with biological material, particularly the most abundant liquid water [3]. These codes include PARTRAC, KURBUC, CPA100 and Geant4-DNA [4]. PARTRAC provides options for simulating the different radiation interaction stages in water targets, such as DNA damage and repair [5]. KURBUC [4] and CPA100 [6] simulate the physical and chemical stages of electron interaction in water and CPA100 can additionally track electrons in DNA material [7, 8]. The Geant4-DNA simulation toolkit [9-12], the low-energy physics extension of the open source Geant4 toolkit [13-15], tracks electrons during the physical stage in liquid water as well as in the chemical stage up to 1 μ s after the first impact to model water radiolysis [16].

Track structure codes consider that the biological medium mainly consists of water since water constitutes up to 70% of living beings. Therefore, simulation studies on DNA damage available in the literature estimate the damages from particle-water interaction [5, 17, 18]. In addition, considering the medium homogeneously filled with liquid water simplifies the calculations and gives a good assumption for an overall dose estimation. However, for DNA damage calculation, this may not be very accurate since the DNA density is higher than water [19] and the probability for particle-DNA interaction is also higher as shown by particle-DNA interaction cross section values [20]. This limitation motivates the need for more accurate particle-DNA interaction simulations.

A recent work by Zein *et al.* [20] introduced a new development of the Geant4-DNA toolkit to extend the “option 6” physics constructor to electrons in DNA nucleobases. This constructor, which is publicly available for liquid water in the 11 eV – 256 keV energy range

98 [21], is based on the CPA100 Fortran-code written by Terrissol *et al.* [6] for electron
99 interactions. CPA100 not only tracks electrons in water but also in DNA constituents: the
100 nucleobases adenine, thymine, guanine and cytosine as well as deoxyribose sugar and the
101 phosphate group [22]. In the recent extension of the “option 6” physics models, interaction
102 cross-sections of electrons with the four nucleobases were calculated for elastic scattering,
103 electronic excitation, and ionisation over the 11 eV - 1 MeV energy range, where they showed
104 good agreement with experiments and calculations reported in the literature. Electronic
105 stopping power, continuous slowing down approximation (CSDA) range and inelastic mean
106 free path were calculated using the cross-sections’ implementation in Geant4-DNA [20].
107

108 In this study, we are complementing this previously published work by calculating the
109 electron cross-sections over the 11 eV - 1 MeV energy range in the deoxyribose and phosphoric
110 acid (bound state of the phosphate group), which constitute the backbone of the DNA molecule.
111 This allowed us to provide a complete set of electron interaction cross-sections for DNA in
112 addition to those previously available for liquid water. While extending the “option 6”
113 constructor, we noticed that the excitation interaction for the four nucleobases was not being
114 adequately sampled and upon testing we noticed that the electron ranges were affected for very
115 low energies only. Therefore, after fixing the bug in the code, we have recalculated the CSDA
116 range of electrons in the four nucleobases and we are presenting the corrected results in this
117 work in addition to the newly introduced values in deoxyribose and phosphoric acid. It is also
118 worth noting that, with the increasing number of materials, the size of the cross-section tables
119 become large, especially regarding the differential cross sections for ionisation. Furthermore,
120 since the number of energy shells of the various organic molecules is very high (for example,
121 36 energy shells for deoxyribose), for each incident electron energy we would need to know
122 the value of the cumulated ionisation probability of each shell to determine the secondary
123 electron energy of emission. In other words, we would need to use large cross-section tables.
124 Hence, in this work we are also introducing a novel sampling method to calculate the
125 transferred secondary electron energy by means of an analytical sampling technique instead of
126 applying the interpolation method from the differential ionisation cross section tables currently
127 used in Geant4-DNA.
128

129 II. Materials and Methods:

130 a) Implementation of the physics model classes

131
132
133 Three new interaction model classes for elastic scattering, excitation and ionisation of
134 electrons were implemented as Geant4-DNA physics models inherited from the G4VEmModel
135 class [10]. Each model class tracks electrons in seven different materials (adenine, thymine,
136 cytosine, guanine, deoxyribose, phosphoric acid, and liquid water) based on their total electron
137 interaction cross sections. The energy range of incident electrons goes from 11 eV to 1 MeV
138 for all materials, except for liquid water, which remains in the 11 eV - 256 keV energy range
139 as in the previous implementation [21]. The total and differential cross section data tables for
140 adenine, thymine, cytosine and guanine were calculated in a previous work [20], while, for
141 deoxyribose and phosphoric acid, the calculations will be described in the following sections.
142 Interpolation between consecutive energy points in the cross-section data tables was applied
143 and electrons were tracked down to 11 eV, where tracks are killed and their energies were
144 deposited locally. The scattering angle is randomly sampled according to the elastic angular
145 differential cross section tables. The transferred energy by ionisation is randomly sampled
146 according to the ionisation energy differential cross section tables. In addition, a new analytical
147

148 sampling method introduced in the following section has also been implemented, which allows
149 the sampling of the transferred energy values as an alternative to the interpolation method.
150 CSDA range and electronic stopping power were calculated using the Geant4-DNA examples
151 “range” and “spower” [12] to verify the model classes and were then compared to data reported
152 in the literature. A comparison between the interpolation and sampling methods was also
153 carried out.

154

155 b) Physics models and cross-sections

156

157 For each mentioned process, the calculations of the cross sections for deoxyribose and
158 phosphoric acid were based on the same models that we used for the four nucleobases adenine,
159 thymine, cytosine and guanine and that are detailed in the previous paper by Zein *et al.* [20]
160 for the same energy range [11 eV – 1 MeV].

161

162 *Elastic scattering*

163

164 The angular differential cross section at a certain incident energy is calculated using the
165 independent atom model (IAM). This model required the internuclear distances between the
166 atoms of the examined molecule, the angular differential cross section of each atom and the
167 complex scattering amplitudes (see equation 1 in paper [20]).

168

169 For atoms, the scattering amplitudes and the differential cross sections were obtained
170 from the Elastic Scattering of Electrons and Positrons by neutral Atoms (ELSEPA) code
171 developed by Salvat *et al.* [23].

172

173 The structures of the considered molecules were obtained through geometry
174 optimizations at Hartree-Fock/cc-pVTZ level, which were performed using the quantum
175 chemistry package *Gaussian09* [24].

176

177 *Ionisation*

178

179 This process required the energy differential cross section for each molecular orbital
180 and the corresponding integrated ionisation cross section over the ejected energy range in order
181 to know which shell was concerned by this process and what was the energy transferred to the
182 ejected electron. To this purpose, the Relativistic Binary Encounter Bethe Vriens (RBEBV)
183 model was used [25]. The analytical forms (equations 2 and 4 in Zein *et al.* [20]) only depend
184 on three parameters, which are representative of each molecular orbital and are determined
185 from the molecular electronic structure. To accomplish this task, the molecular orbitals of each
186 molecule were obtained through *ab initio* quantum chemistry calculations at restricted Hartree-
187 Fock/cc-pVTZ level on the above-mentioned optimized molecular geometries using the
188 GAMESS-UK software [26], as already done for the four DNA nucleobases in the previous
189 paper by Zein *et al.* [20].

190

191 For deoxyribose, there are 36 molecular orbitals including 9 inner shells, while, for
192 phosphoric acid, we have 25 molecular orbitals with 9 inner shells. The energy threshold varies
193 from 11.24 eV to 559.77 eV for deoxyribose and from 13.00 eV to 2179.56 eV for phosphoric
194 acid.

195

196

197

198
199
200
201
202

Table 1. Ionisation and excitation outer shell binding energy:

Binding energy (eV)	Water	Adenine	Cytosine	Guanine	Thymine	Deoxyribose	Phosphoric acid
Ionisation	10.79	8.51	9.32	8.23	9.64	11.24	13.00
Excitation	8.17	8.51	9.32	8.23	9.64	11.24	13.00

203
204
205
206

Excitation

207 The total excitation cross section was linked to the total ionisation cross section and to
208 the ratio of the total excitation over ionisation cross section in water at a given incident energy,
209 as it was proposed in the initial version of the CPA100 code [6].

210
211
212
213

With the assumption that only electronic levels lower than 20 eV can be excited, we considered 17 excitation levels for deoxyribose and 9 for phosphoric acid. We assumed that each level had the same probability to be chosen.

214
215

c) Sampling Method

216
217
218
219
220

Following the Relativistic Binary Encounter Bethe Vriens (RBEBV) model for each molecular orbital from the threshold to 1 MeV, the relativistic energy differential cross section written in the reduced form is (equation 2 in paper Zein *et al.* [20])

$$\frac{d\sigma}{dw} = \frac{4\pi a_0^2 \alpha^4 N}{(\beta_t^2 + \beta_u^2 + \beta_b^2) 2b'}$$

$$\cdot \left[-\frac{\phi}{t+1} \cdot \left(\frac{1}{w+1} + \frac{1}{t-w} \right) \cdot \frac{1+2t'}{(1+t'/2)^2} + \frac{1}{(w+1)^2} + \frac{1}{(t-w)^2} \right. \\ \left. + \frac{b'^2}{(1+t'/2)^2} + \left(\text{Ln} \left(\frac{\beta_t^2}{1-\beta_t^2} \right) - \beta_t^2 - \text{Ln}(2b') \right) \cdot \left(\frac{1}{(w+1)^3} + \frac{1}{(t-w)^3} \right) \right] \quad (1)$$

221
222

With $w = \frac{W}{B}$

$$\beta_t^2 = 1 - \frac{1}{(1+t')^2} \quad \text{and} \quad t' = \frac{T}{mc^2} \quad \text{and} \quad t = \frac{T}{B}$$

$$\beta_u^2 = 1 - \frac{1}{(1+u')^2} \quad \text{and} \quad u' = \frac{U}{mc^2} \quad \text{and} \quad u = \frac{U}{B}$$

$$\beta_b^2 = 1 - \frac{1}{(1+b')^2} \quad \text{and} \quad b' = \frac{B}{mc^2}$$

223

224 where α , m and c are the fine structure constant, the electron mass and the speed of light in
 225 vacuum, respectively.

226

227 T is the incident electron kinetic energy and W is the ejected electron kinetic energy. B
 228 (i.e., the bound electron binding energy), U (i.e., the bound electron kinetic energy), and N (i.e.,
 229 the occupation number of the subshell to be ionized) are the three parameters representative of
 230 the molecular shell.

231

The relativistic form of the Vriens function ϕ is written as
$$\phi = \cos \left[\sqrt{\frac{\alpha^2}{(\beta_t^2 + \beta_b^2)}} \text{Ln} \left(\frac{\beta_t^2}{\beta_b^2} \right) \right]$$

232 To sample the reduced kinetic energy of the secondary electron w , the composition
 233 sampling method already used for the non-relativistic BEB version in liquid water (Bordage *et*
 234 *al.* [21]) was expanded and adapted for the DNA constituents. The equation must be written as
 235 the sum of positive functions of w , denoted $k_i(w)$:

$$\frac{d\sigma}{dw} = k_1(w) + k_2(w) + k_3(w) \quad (2)$$

236 The functions k_i can be decomposed as the product of three terms (A_i , h_i and g_i):

$$k_i(w) = A_i \cdot h_i(w) \cdot g_i(w) \quad (3)$$

237 which satisfy the following constraints

$$G_i = \int_0^{\frac{t-1}{2}} g_i(w) dw = 1$$

$$\text{and } \forall w : \begin{cases} 0 \leq h_i(w) \leq 1 \\ g_i(w) \geq 0 \\ \exists G_i, G_i^{-1} \\ A_i \geq 0 \end{cases} \quad (4)$$

238

239 In order to respect these constraints, the k_i functions (eq 3) are written as

240

$$241 \quad k_1(w) = \frac{4\pi a_0^2 \alpha^4 N}{(\beta_t^2 + \beta_u^2 + \beta_b^2) 2b'} \cdot \left(\frac{1}{(w+1)^2} - \frac{\phi D}{(t+1)(w+1)} - \frac{\phi D}{2(t+1)(t-w)} + F \right)$$

$$242 \quad k_2(w) = \frac{4\pi a_0^2 \alpha^4 N}{(\beta_t^2 + \beta_u^2 + \beta_b^2) 2b'} \cdot \left(\frac{1}{(t-w)^2} - \frac{\phi D}{2(t+1)(t-w)} \right)$$

$$243 \quad k_3(w) = \frac{4\pi a_0^2 \alpha^4 N}{(\beta_t^2 + \beta_u^2 + \beta_b^2) 2b'} \cdot \frac{1}{(w+1)^3} \cdot \left(1 + \left(\frac{w+1}{t-w} \right)^3 \right)$$

$$244 \quad \cdot \left(\text{Ln} \left(\frac{\beta_t^2}{1 - \beta_t^2} \right) - \beta_t^2 - \text{Ln}(2b') \right)$$

245

$$246 \quad \text{where } D = \frac{1+2t'}{(1+t'/2)^2} \text{ and } F = \frac{b'^2}{(1+t'/2)^2}$$

247

248 Each term of equation 3, fulfilling the constraints expressed through equation 4, can
 249 be decomposed as follows:

250

251 For the first function (k_1), we have:

$$252 A_1 = \frac{4\pi a_0^2 \alpha^4 N}{(\beta_t^2 + \beta_u^2 + \beta_b^2) 2b'} \cdot \frac{t-1}{t+1} \cdot \frac{(1+F)2t(t+1) - \phi D(2t+1)}{2t(t+1)}$$

253

$$254 g_1(w) = \frac{t+1}{t-1} \frac{1}{(w+1)^2};$$

255

$$256 h_1(w) = \left[1 - \frac{\phi D(w+1)}{(t+1)} \left(1 + \frac{(w+1)}{2(t-w)} \right) \right. \\ \left. + F(w+1)^2 \right] \cdot \frac{2t(t+1)}{(1+F)2t(t+1) - \phi D(2t+1)}$$

257

258 For the second one (k_2):

$$259 A_2 = \frac{4\pi a_0^2 \alpha^4 N}{(\beta_t^2 + \beta_u^2 + \beta_b^2) 2b'} \cdot \frac{t-1}{t(t+1)} \frac{4 - \phi D}{4}$$

260

$$261 g_2(w) = \frac{t(t+1)}{t-1} \frac{1}{(t-w)^2};$$

262

$$263 h_2(w) = \left(1 - \frac{\phi D(t-w)}{2(t+1)} \right) \cdot \frac{4}{4 - \phi D}$$

264

265 and for the third one (k_3):

$$266 A_3 = \frac{4\pi a_0^2 \alpha^4 N}{(\beta_t^2 + \beta_u^2 + \beta_b^2) 2b'} \cdot \left(\text{Ln} \left(\frac{\beta_t^2}{1 - \beta_t^2} \right) - \beta_t^2 - \text{Ln}(2b') \right) \frac{(t+1)^2 - 4}{(t+1)^2}$$

267

$$268 g_3(w) = \frac{2(t+1)^2}{(t+1)^2 - 4} \cdot \frac{1}{(w+1)^3}$$

269

$$h_3(w) = \frac{1}{2} \left(1 + \left(\frac{w+1}{t-w} \right)^3 \right)$$

270

271 The $g_i(w)$ functions were defined in order for the cumulative distribution function
272 G_i to exist and to have an inverse function.

273

274 Furthermore, as it was developed in the appendix of the paper by Bordage *et al.* [21], two
275 steps are required for the sampling:

276

277 a- The generation of the first random number, R_1 , to select which k_i function should be
278 sampled, such as:

$$279 \sum_{i=1}^{k-1} A_i \leq R_1 \leq \sum_{i=1}^k A_i$$

280

281 b- Once the k_i function is chosen, the generation of a second random number R_2 to
generate the energy loss w_x with respect to the probability density g_i , so that $\int_0^{w_x} g_i(w) dw = R_2$
and w_x is rejected if $R_3 > h_k(w_x)$

282

283

284

285 III. Results:

286

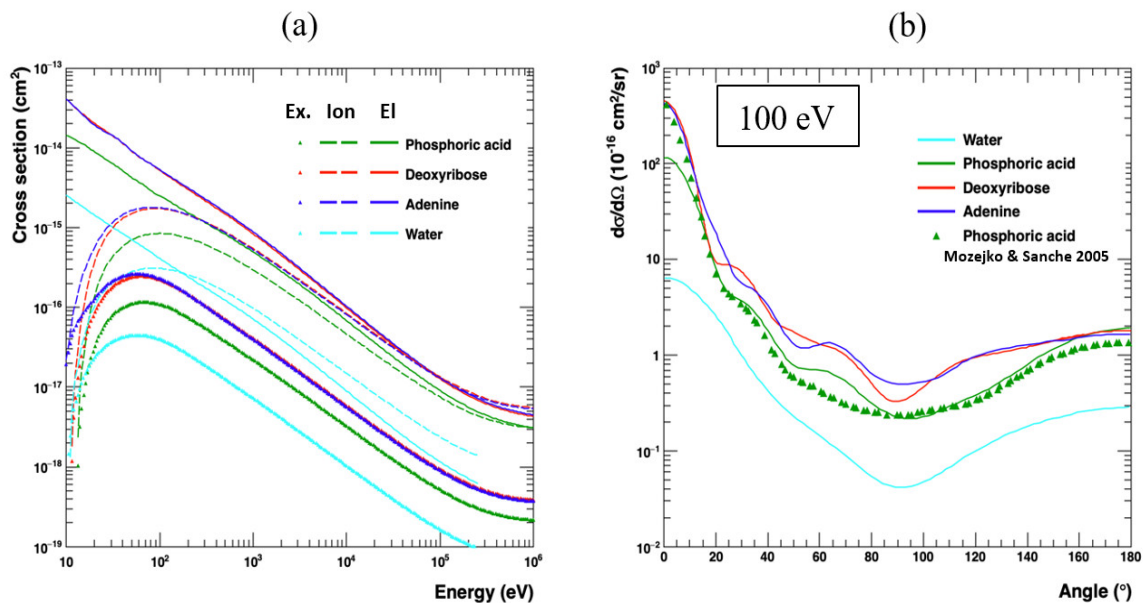
287 a) Total Cross Sections of deoxyribose and phosphoric acid:

288

289 Figure 1 (a) shows the calculated total cross sections as a function of the electron
290 incident energy for the three processes (elastic scattering, excitation and ionisation) and for the
291 two studied materials (deoxyribose and phosphoric acid). For comparison, the curves for
292 adenine [20] and liquid water-option6 [21] implemented in Geant4-DNA are also plotted. The
293 results for adenine and deoxyribose are very close and are higher than those for phosphoric
294 acid for all incident energies.

295 As an example, Figure 1 (b) shows the variation of the differential elastic cross section
296 as a function of the scattering angle at an incident energy of 100 eV for phosphoric acid and
297 deoxyribose. The results are compared with differential cross section in adenine and water, as
298 well as with the only published calculations at this energy by Mozejko and Sanche [27].
299

299



300

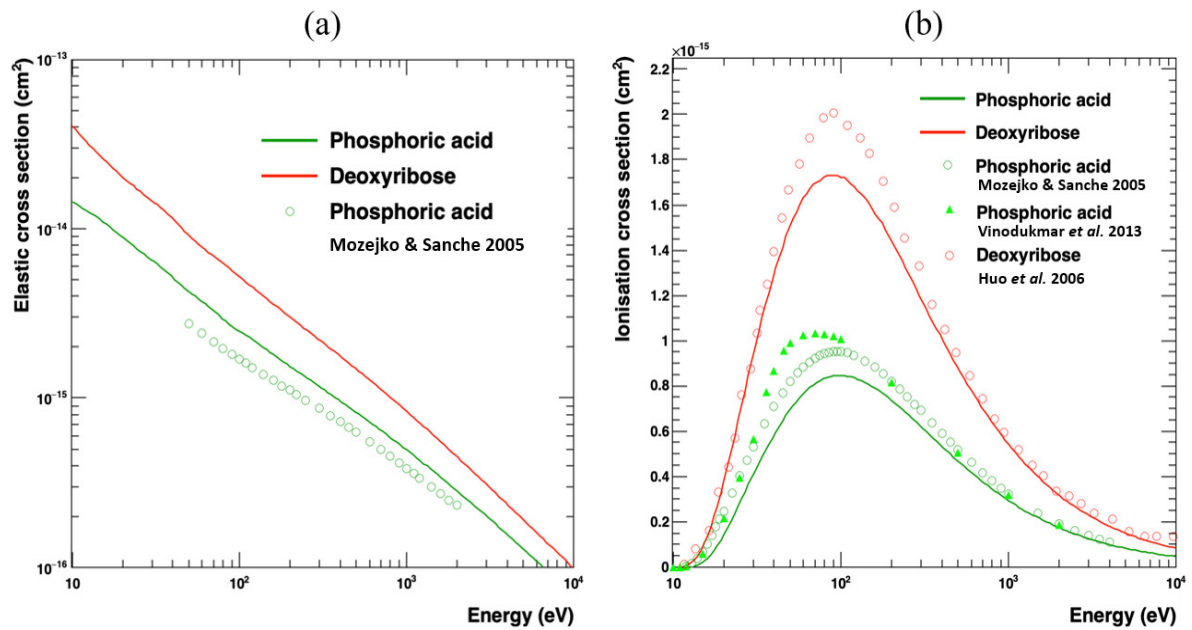
301 *Figure 1. (a) Total cross sections for elastic scattering (El), excitation (Ex) and ionisation (Ion)*
302 *for deoxyribose and phosphoric acid compared to adenine [20] and water-option6 [21].*

303 *(b) Differential elastic cross section for incident energy of 100 eV for deoxyribose and*
304 *phosphoric acid, compared to adenine [20] and liquid water-option6 [21] and the published*
305 *calculated data by Mozejko and Sanche [27] for phosphoric acid.*

306

307

308 Figure 2 (a) shows the total elastic cross sections of deoxyribose and phosphoric acid
309 as a function of the incident energy. The comparison with the work of Mozejko on phosphoric
310 acid [27] is also shown. In Figure 2 (b) the total ionisation cross sections of deoxyribose and
311 phosphoric acid are depicted and compared with published data reported in the literature [27-
312 29]. There are no other theoretical or experimental data for cross sections of phosphoric acid
313 and deoxyribose available for comparison.



314

315 *Figure 2. Comparison of the present cross sections (continuous lines) with calculations from*
 316 *the literature (symbols) (a) for elastic scattering in phosphoric acid done by Mozejko and*
 317 *Sanche [27], and (b) for the total ionisation cross section in deoxyribose done by Huo et al.*
 318 *[28] and phosphoric acid done by Mozejko and Sanche [27] and by Vinodukmar et al. [29].*

319

320 b) Range

321

322

323

324

325

326

327

328

329

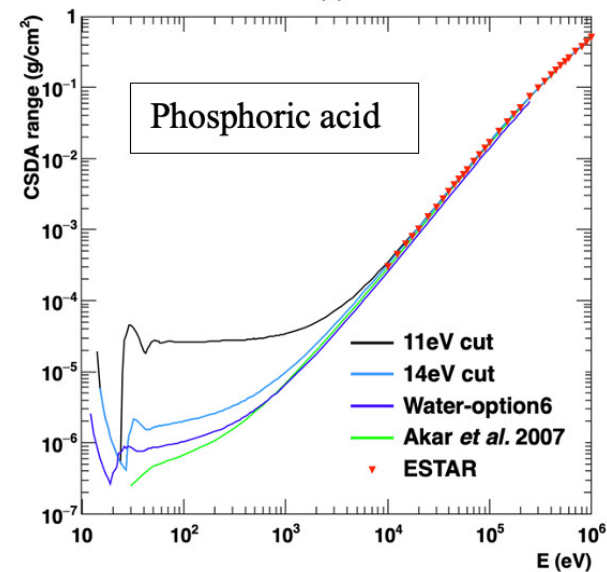
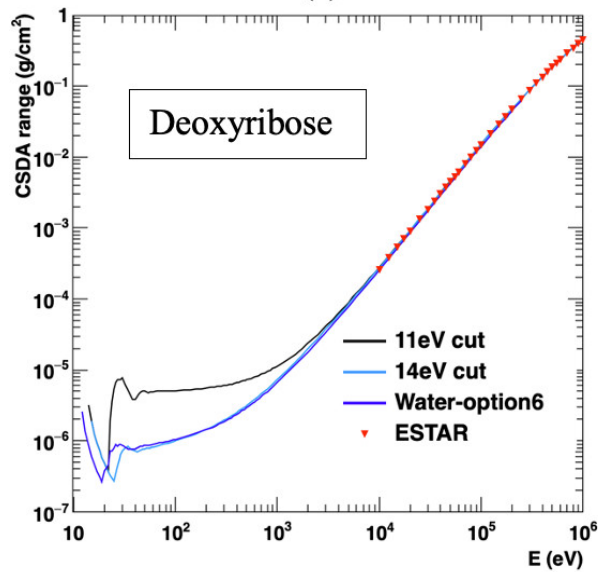
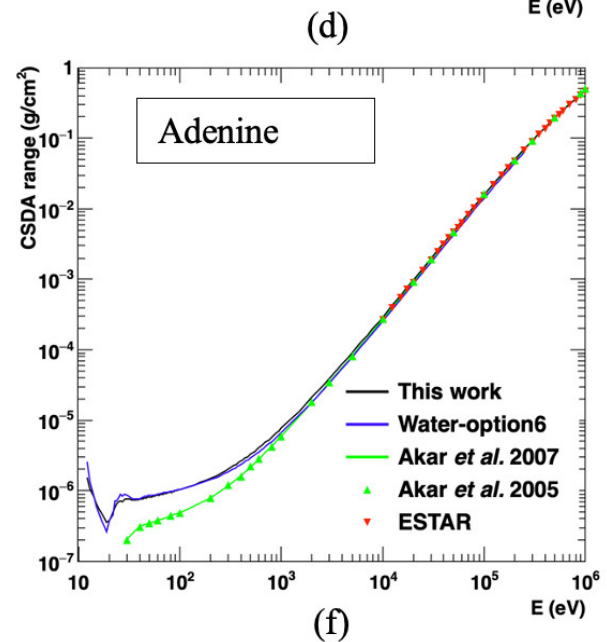
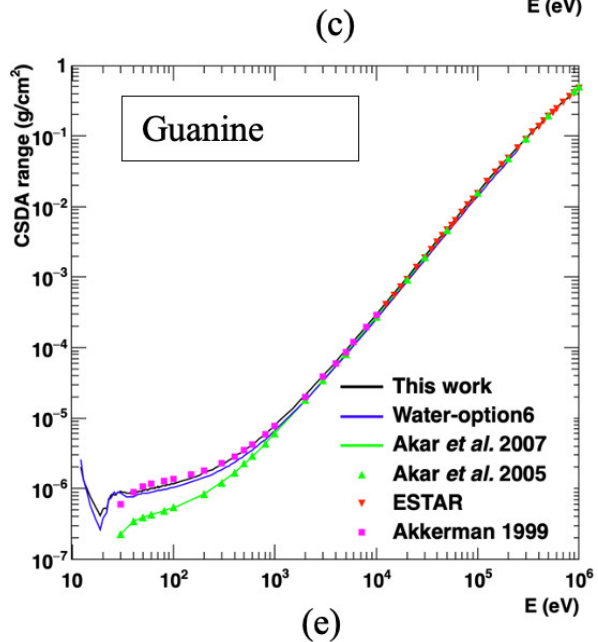
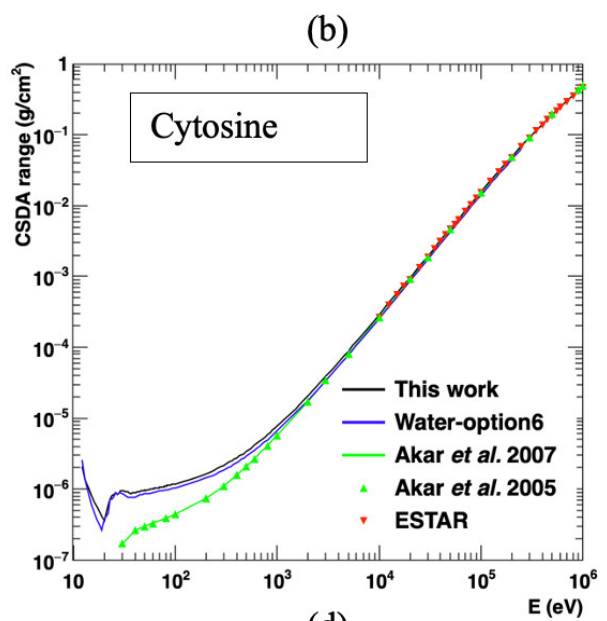
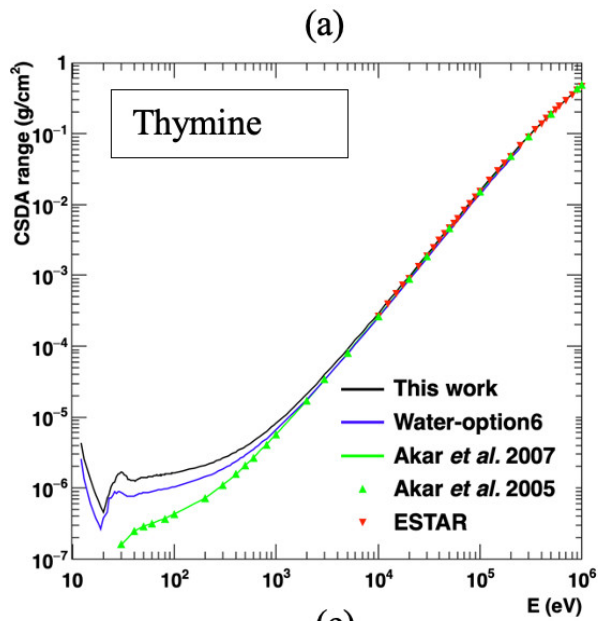
330

331

332

333

Figure 3 shows the range in all materials as calculated using the updated version of the “option 6” physics models over the 11 eV – 1 MeV energy range (11 eV – 256 keV for liquid water). The comparison with calculations reported in the literature shows a good agreement for energies higher than 1 keV, while for the comparison with liquid water we can observe some differences at low energies (< 1keV). Figures 3 (e) and (f) show the range in deoxyribose and phosphoric acid calculated with a low energy cut of 14 eV, below which the energy was deposited locally. Since the excitation and ionisation energy levels of deoxyribose and phosphoric acid are higher than the low energy limit 11 eV, the 14 eV cut was tested as the first energy above the inelastic outer shell binding energies (see Table 1). This indicates that the range is affected by elastic scattering at low sub-inelastic energies of deoxyribose and phosphoric acid (Table 1).

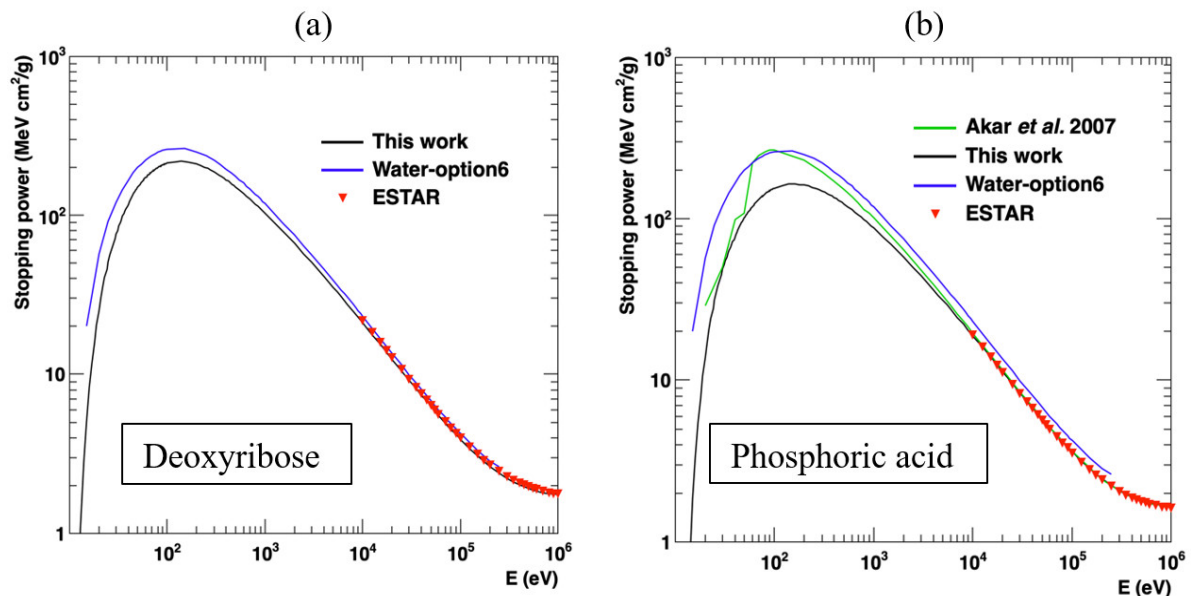


335 Figure 3. CSDA range calculated for (a) thymine, (b) cytosine, (c) guanine, (d) adenine, (e)
 336 deoxyribose and (f) phosphoric acid in Geant4-DNA and compared to water “option 6” [21],
 337 data from the literature (Akar et al. 2005 [30], Akar et al. 2007 [31], Akkerman 1999 [32])
 338 and the ESTAR database [33]. Panels (a), (b), (c), and (d) show the ranges calculated with 11
 339 eV cut (black curves) which is the lowest value in the implemented energy range. Panels (e)
 340 and (f) show the effect of the energy cut-off on the range calculation with 11 eV cut (in black)
 341 set at the low energy limit and 14 eV cut (in light blue) just above the first ionisation level of
 342 phosphoric acid.

343
 344 a) Stopping Power

345
 346 Figure 4 shows the electronic stopping power calculation in deoxyribose and
 347 phosphoric acid in comparison with the work of Akar 2007 *et al.* [31], which is currently the
 348 only available calculation in the literature for phosphoric acid. We also compared with
 349 calculations from the ESTAR database [33], which depend on the densities and the chemical
 350 formula of the deoxyribose ($C_5H_{10}O_4$) and phosphoric acid (H_3PO_4). Densities and chemical
 351 formulas for each material are given in Table 2.

352



353
 354 Figure 4. Electronic stopping power calculated for (a) deoxyribose and (b) phosphoric acid in
 355 Geant4-DNA and compared to water-option 6 [21], data from the literature calculated by Akar
 356 *et al.* [31] and the ESTAR database [33].

357

358

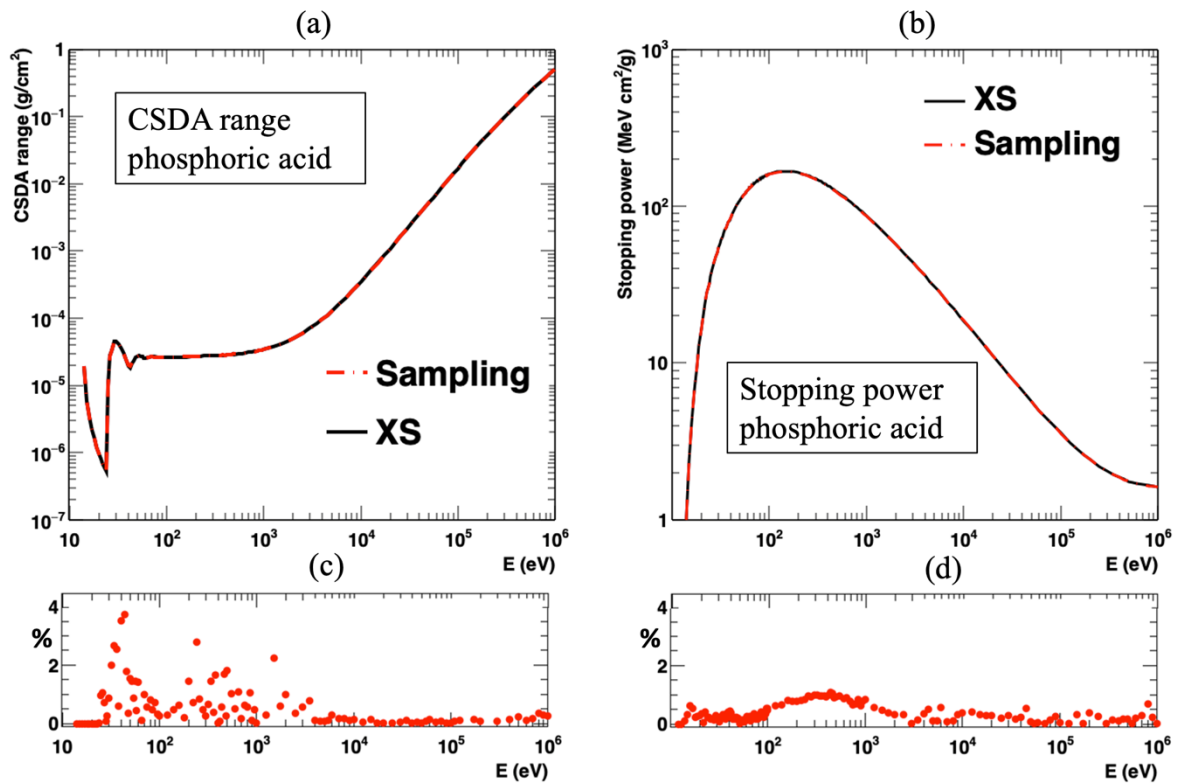
359

360 c) Comparison of interpolation and sampling methods:

361

362 Figure 5 shows the range and electronic stopping power of electrons in phosphoric acid
 363 calculated using the method based on the interpolation of tabulated cross section data and the
 364 sampling method. The same test was performed for the other materials and the difference
 365 between the sampling and interpolation methods was less than 1.5% difference in stopping
 366 power and less than 4% difference in range for all the six examined materials.

367



368
369

370 *Figure 5. (a) CSDA range and (b) stopping power of phosphoric acid calculated with sampling*
 371 *and interpolation (XS) methods of ionisation differential cross sections. Panels (c) and (d)*
 372 *show the absolute percentage difference of range and stopping power by the sampling method*
 373 *relative to the interpolation method.*

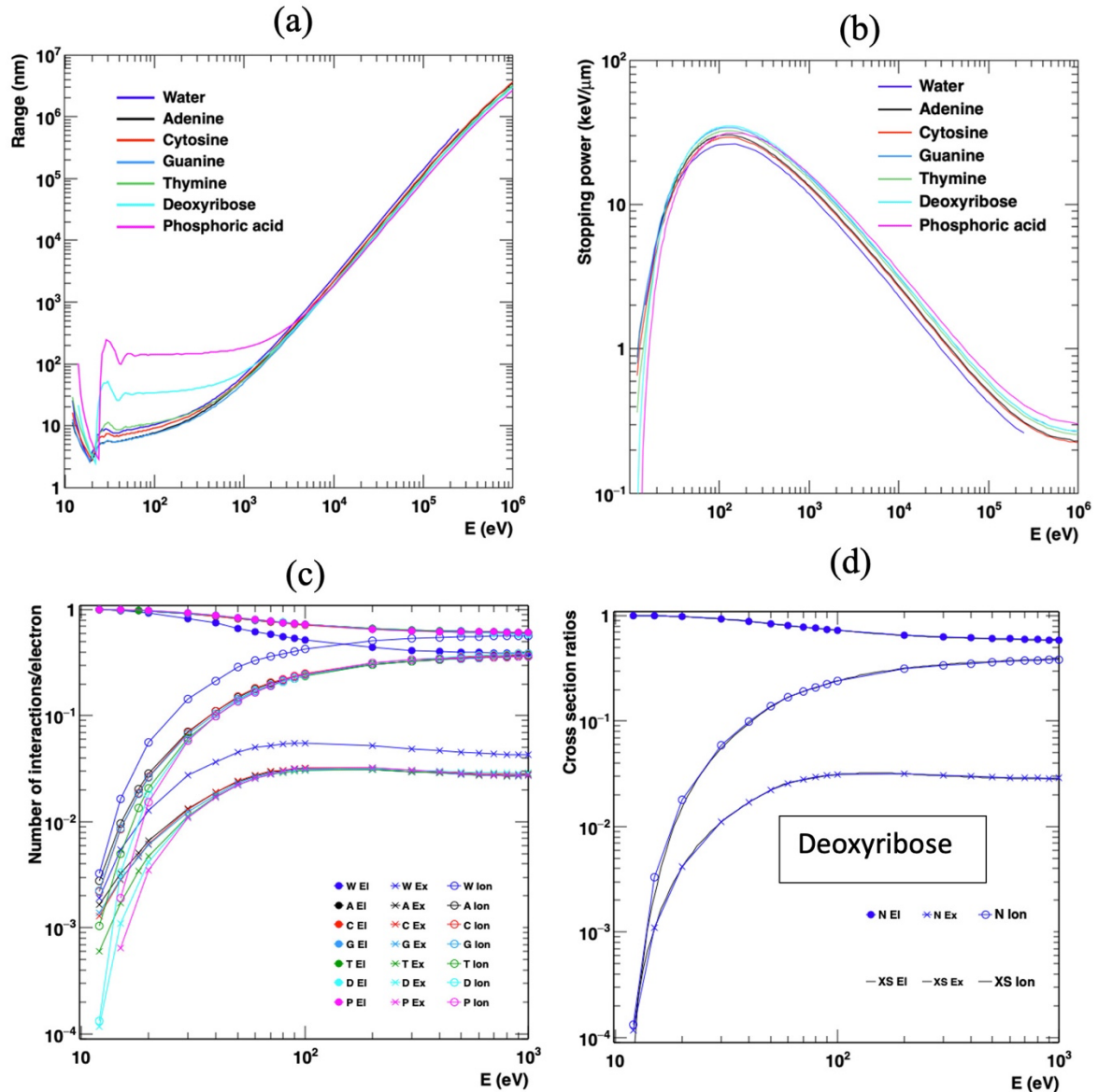
374
375

376 d) Interaction type ratio

377

378 In Figure 6 (a) the CSDA range of electrons in all 7 materials with 11 eV cutoff is
 379 shown. Phosphoric acid and deoxyribose have larger ranges at energies lower than 10 keV
 380 compared to the other materials due to their high contribution of elastic scattering in the sub-
 381 inelastic range. The CSDA range shows direct dependence on the density of the materials for
 382 energies above 10 keV. Figure 6 (b) shows the electronic stopping power in all the materials
 383 under study. Above 200 eV, the stopping power is directly proportional to the density of the
 384 material while for the lower energies the interaction cross-sections influence the stopping
 385 power. In Figure 6 (c) the ratio of the three interactions per electron event as a function of
 386 energy is calculated. Only the first interaction was registered per incident electron event, and
 387 the total number of interaction types was calculated and then normalized to the total number of
 388 events. 10^6 events were tested per material. This calculation reflects the interaction type
 389 probability to occur per electron energy. The cross-section type ratio to the total cross section
 390 by all the three interactions in deoxyribose is shown in Figure 6 (d) in comparison to the ratio
 391 between the number of interaction types and the total number of interactions per incident
 392 electron. As expected, the calculated ratio of interactions from the simulations agrees well with
 393 the ratio of cross sections for all three types of interactions. The same results were found for
 394 all the materials under investigation (for the sake of simplicity, only deoxyribose is shown
 395 here), which assures the correct implementation of the interaction models in the simulation.

396



397
 398 *Figure 6. (a) CSDA range of the 7 different materials with 11 eV low energy cutoff. (b)*
 399 *Electronic stopping power of the 7 different materials. (c) Ratio of the number of interactions*
 400 *per incident electron in the 7 different materials. Legend symbols: W (Water), A (adenine), C*
 401 *(cytosine), G (guanine), T (thymine), D (deoxyribose), P (phosphoric acid), El (elastic*
 402 *scattering), Ex (excitation), Ion (ionisation). (d) Ratio of the number of interactions per*
 403 *incident electron in comparison with the cross-section ratios of deoxyribose. Legend symbols:*
 404 *N (number of interactions/incident electron) and XS (cross section type ratio to the total cross*
 405 *section of all 3 interactions).*

406
 407
 408
 409

Table 2. Chemical formulas and densities of the materials [19, 34, 35]

	Water	Adenine	Cytosine	Guanine	Thymine	Deoxyribose	Phosphoric acid
Formula	H_2O	$C_5H_5N_5$	$C_4H_5N_3O$	$C_5H_5N_5O$	$C_5H_6N_2O_2$	$C_5H_{10}O_4$	H_3PO_4

Density (g/cm ³)	1	1.35	1.3	1.58	1.48	1.5	1.87
---------------------------------	---	------	-----	------	------	-----	------

410
411
412
413
414
415

IV. Discussion:

416 Monte Carlo track structure codes provide good tools for estimating DNA damages;
417 however, the so far performed Monte Carlo studies on DNA damage considered liquid water
418 as a surrogate of the biological medium and this led to underestimate the damage rate of the
419 DNA molecule itself [5, 17, 18]. This limitation is what motivated our previous work, where
420 we introduced new calculations of electron interaction cross sections in the four DNA bases
421 for elastic scattering, excitation and ionization [20]. These cross sections were used in the
422 implementation of new physics models of electrons for the purpose of extending the Geant4-
423 DNA toolkit tracking capabilities in the DNA material. In this work, the electron interaction
424 cross sections in the deoxyribose sugar and the phosphoric acid are calculated to complete the
425 physics models in all DNA components.

426

427 The total cross sections of the three electron interactions, elastic scattering, excitation
428 and ionization, with all DNA material are higher than those of liquid water, as shown in our
429 previous work [20] and in Figure 1(a). Cross sections of deoxyribose are very close to those of
430 adenine; however, they are higher than those of phosphoric acid for all incident energies. In
431 addition, the densities of the DNA components are higher than liquid water as shown in Table
432 2. Therefore, the rate of particle with DNA interaction is expected to be higher than the one
433 with water interaction, which emphasizes the inaccuracy of substituting water for DNA at the
434 sub-cellular scale in Monte Carlo simulation studies.

435

436 The limited data available in the literature for this type of calculations makes it difficult
437 to perform thorough comparisons, specifically for the deoxyribose and the phosphate. The only
438 available elastic scattering cross section data in the literature are limited to theoretical values
439 for phosphoric acid. Differential and integrated cross sections are calculated at energies
440 between 50 eV and 2 keV by Mozejko and Sanche [27]. The present integrated elastic cross
441 sections values are higher than those of reference [27] (Figure 2 (a)). Comparison of elastic
442 differential cross section for phosphoric acid at 100 eV shows an overall good agreement with
443 the calculations of Mozejko and Sanche for most scattering angles, with lower values at very
444 small scattering angles ($< 20^\circ$) (Figure 1 (b)). The data between 0 and 25 eV (Winstead et
445 McKoy [36], Tonzani and Greene [37]) are not included.

446 For ionisation, we can compare only the total cross section (sum of the contribution of
447 each orbital) with the only available theoretical results of Huo *et al.* [28] based on BEB method
448 for deoxyribose, and for phosphoric acid with two different calculations (Mozejko and Sanche
449 [27] and Vinodkumar *et al.* [29]). The results are in a relatively good agreement except in the
450 energy range lower than 100 eV for phosphoric acid. Moreover, the present data are lower than
451 those resulting from other calculations (Figure 2 (b)).

452

453 During the extension of these models previously implemented for the four DNA
454 nucleobases [20], a bug was identified on the sampling of excitation, which affects only the
455 range results at very low energy but neither the stopping power nor the inelastic mean free path.
456 Therefore, after fixing the bug in the code, in this manuscript we decided to include the updated

457 range figures for the four DNA nucleobases adenine, thymine, guanine and cytosine (see panels
458 a, b, c and d in Figure 3).

459

460 At high energy, a good agreement in range is observed with the published data, with a
461 deviation at low energy (<1 keV) for all four nucleobases. The range is different than the one
462 obtained from the liquid water calculation through Geant4-DNA using the same lower cutoff
463 energy of 11 eV for all materials and the same physics models of the “option6” Geant4-DNA
464 constructor. The new update affects the range curve at energies lower than 1 keV, where the
465 CSDA range of the four nucleobases are closer to that of liquid water. Note that the range
466 curves are normalized to the density of the material. At very low energy (<100 eV), thymine
467 shows higher CSDA range values than adenine, cytosine and guanine, (see Figure 6 (a)) which
468 is due to the lower inelastic cross sections of thymine compared to adenine, cytosine and
469 guanine for energies less than 30 eV. This results in an elevated number of elastic scattering
470 interactions at low energies. Because of the higher occurrence probability of elastic scattering,
471 elastic scattering becomes highly dominant compared to excitation and ionisation, thus leading
472 to longer electron tracks and, consequently, to a higher range (Figure 3 (a)). This can also be
473 seen in Figure 6 (c), where excitation and ionisation probabilities of thymine are lower than
474 adenine, cytosine and guanine for energies lower than 30 eV, consequently leading to a greater
475 dominance of elastic scattering.

476

477 Deoxyribose and phosphoric acid have the outermost binding energy values, in
478 particular higher than the tracking energy cutoff of 11 eV (11.24 eV for deoxyribose and 13
479 eV for phosphoric acid, Table 1). Therefore, when an electron reaches energies below the
480 binding energy threshold, only elastic scattering takes place and leads to long electron tracks
481 without significant energy loss. This significantly affects the CSDA range of phosphoric acid
482 and, to a lesser extent, the CSDA range of deoxyribose for low energies (< 1 keV), as shown
483 in Figures 3 (e) and (f) also Figure 6 (a). Similar to thymine, deoxyribose and phosphoric acid
484 have lower inelastic probabilities at energies lower than 30 eV (Figure 6 (c)), which also
485 contributes to the high CSDA range at low energies. When calculating the range with a 14 eV
486 energy cutoff for deoxyribose and phosphoric acid, which is higher than the lowest binding
487 energy of phosphoric acid, the range dramatically decreases and becomes closer to water at
488 very low energies due to the higher contribution of the inelastic processes and the limited effect
489 of elastic scattering. Because of the high binding energies of the DNA backbone components,
490 one should pay attention to the energy cutoff used for simulations, which might affect the
491 results.

492

493 Stopping power calculations of both deoxyribose and phosphoric acid show a good
494 agreement with the very scarce data from the literature, and an obvious difference from the
495 liquid water calculations of Geant4-DNA is observed over the entire energy range (Figure 4).
496 For low energies, the phosphoric acid has a lower collision stopping power than the one
497 resulting from the calculations performed by Akar *et al.* [31]. The peak in this work is reached
498 at 120 eV compared to 80 eV in the work by Akar and coworkers.

499

500 The sampling method introduced in this work allows efficient calculations of the
501 secondary transferred energy after ionisation interaction. The conventional way through which
502 Geant4-DNA calculates the secondary electron kinetic energy currently uses an interpolation
503 method that samples the energy from tabulated data and applies an interpolation function that
504 estimates the energy from two consecutive values corresponding to an ionisation shell. This
505 normally requires a differential cross sections table file providing the incident energy intervals
506 as well as the corresponding cumulative distribution of energy loss for each ionisation shell.

507 Since the incident energy range is extended up to 1 MeV and the biological molecules have a
508 high number of ionisation shells (> 29) compared to liquid water (5 ionisation shells), the
509 required data files become large to handle, build and distribute within the Geant4 toolkit.
510 Therefore, the sampling method provides a convenient solution without affecting the outcome
511 of the simulation results. In addition, calculating the transferred energy directly within the code
512 represents a more accurate method than interpolation between two consecutive energy values,
513 which may introduce some variation if the difference between the two energies is not
514 sufficiently small. The differences between the sampling and the interpolation methods showed
515 a maximum of 4% for CSDA range calculations and less than 2% for collision stopping power
516 computations for all materials (Figures 5 (c) and (d)). However, the sampling method does not
517 have any advantage over the interpolation concerning the computational cost. A similar method
518 based on the binary encounter Bethe model was already introduced and is currently available
519 for liquid water [21]. The sampling routine can also be applied with materials for which the
520 relativistic binary encounter Bethe relativistic energy differential cross sections are used
521 (equation 1). For the moment, it could be used directly not only for the four DNA nucleobases
522 [20], deoxyribose and phosphoric acid but also for gold [38]. Another advantage of this work
523 is that the here-presented approach could be exploited in future applications of Geant4-DNA
524 damage models calculation, where the physics constructor “option6” could be used in
525 combination with the detailed DNA geometry introduced by Lampe, especially because we are
526 using the same architecture and chemical composition of the DNA constituents [39, 40].
527
528
529

530 V. Conclusion:

531
532 In this study, an update of the Geant4-DNA physics constructor “option 6” was
533 described. This update includes a full set of electron interaction cross-sections for elastic
534 scattering, electronic excitation and ionisation for the different components of the DNA
535 molecule, in addition to those already available for liquid water. The model has been tested
536 considering CSDA range and stopping power of electrons for the various DNA components,
537 where we observed a good agreement with data available in the literature. In addition, a novel
538 sampling method for calculating the secondary ionisation electrons kinetic energy was
539 introduced, which will reduce the total memory allocated for the ionisation differential cross-
540 section tables.
541

542 This work represents a stepping stone for particle interaction simulations with organic
543 materials not limited to DNA only. The methods and architecture of the physics models can be
544 translated to other molecules, such as amino acids that make up proteins. In combination with
545 detailed geometry, more realistic simulations at the subcellular scale could be achieved, which
546 would lead to better understanding of radiation effects on biological material. The physics
547 models could also be adapted and expanded for the cross-section calculation of other particles,
548 such as protons. The sampling method introduced could be used as an efficient alternative for
549 interpolation methods in future releases of Geant4-DNA. All in all, the complete package of
550 electron interactions in the DNA constituents provides a novel tool for a new generation of
551 Monte Carlo simulations.
552

553 Acknowledgements:

554
555 The authors would like to thank Dr. Dousatsu Sakata for his valuable advice.

556 References:

557
558
559
560
561
562
563
564
565
566
567
568
569
570
571
572
573
574
575
576
577
578
579
580
581
582
583
584
585
586
587
588
589
590
591
592
593
594
595
596
597
598
599
600
601
602
603
604

1. Borges, H.L., R. Linden, and J.Y.J. Wang, *DNA damage-induced cell death: lessons from the central nervous system*. Cell Research, 2008. **18**(1): p. 17-26.
2. Chatterjee, N. and G.C. Walker, *Mechanisms of DNA damage, repair, and mutagenesis*. Environmental Molecular Mutagenesis, 2017. **58**(5): p. 235-263.
3. El Naqa, I., P. Pater, and J. Seuntjens, *Monte Carlo role in radiobiological modelling of radiotherapy outcomes*. Physics in Medicine and Biology, 2012. **57**(11): p. R75-97.
4. Nikjoo, H., et al., *Track-structure codes in radiation research*. Radiation Measurements, 2006. **41**(9): p. 1052-1074.
5. Friedland, W., et al., *Comprehensive track-structure based evaluation of DNA damage by light ions from radiotherapy-relevant energies down to stopping*. Scientific Reports, 2017. **7**: p. 45161.
6. Terrissol, M. and A. Beaudre, *Simulation of space and time evolution of radiolytic species induced by electrons in water*. Radiation Protection Dosimetry, 1990. **31**(1-4): p. 175-177.
7. Edel, S., *Modélisation du transport des photons et des électrons dans l'ADN plasmide*. 2006, PhD Thesis, Université Toulouse III-Paul Sabatier, Toulouse, France.
8. Peudon, A., *Prise en compte de la structure moléculaire pour la modélisation des dommages biologiques radio-induits*. 2007, PhD Thesis, Université Toulouse III-Paul Sabatier, Toulouse, France.
9. Bernal, M.A., et al., *Track structure modeling in liquid water: A review of the Geant4-DNA very low energy extension of the Geant4 Monte Carlo simulation toolkit*. Physica Medica: European Journal of Medical Physics, 2015. **31**(8): p. 861-874.
10. Incerti, S., et al., *The Geant4-DNA Project*. International Journal of Modeling, Simulation, and Scientific Computing, 2010. **01**(02): p. 157-178.
11. Incerti, S., et al., *Comparison of GEANT4 very low energy cross section models with experimental data in water*. Medical Physics, 2010. **37**(9): p. 4692-4708.
12. Incerti, S., et al., *Geant4-DNA example applications for track structure simulations in liquid water: A report from the Geant4-DNA Project*. Medical Physics, 2018. **45**(8): p. e722-e739.
13. Agostinelli, S., et al., *GEANT4—a simulation toolkit*. Nuclear Instruments and Methods in Physics Research A, 2003. **506**(3): p. 250-303.
14. Allison, J., et al., *Geant4 developments and applications*. IEEE Transactions on Nuclear Science, 2006. **53**(1): p. 270-278.
15. Allison, J., et al., *Recent developments in Geant4*. Nuclear Instruments and Methods in Physics Research A, 2016. **835**: p. 186-225.
16. Karamitros, M., et al., *Modeling Radiation Chemistry in Geant4 Toolkit*. Nuclear Science and Technology, 2011. **2**: p. 505 - 508.
17. Friedland, W., et al., *Simulation of DNA damage after proton irradiation*. Radiation Research, 2003. **159**(3): p. 401-10.
18. Francis, Z., C. Villagrasa, and I. Clairand, *Simulation of DNA damage clustering after proton irradiation using an adapted DBSCAN algorithm*. Computer Methods and Programs in Biomedicine, 2011. **101**(3): p. 265-270.
19. Tan, Z., et al., *Proton stopping power in a group of bioorganic compounds over the energy range of 0.05–10MeV*. Nuclear Instruments and Methods in Physics Research Section B: Beam Interactions with Materials and Atoms, 2006. **248**(1): p. 1-6.

- 605 20. Zein, S.A., et al., *Electron transport in DNA bases: An extension of the Geant4-DNA*
606 *Monte Carlo toolkit*. Nuclear Instruments and Methods in Physics Research Section
607 B: Beam Interactions with Materials and Atoms, 2021. **488**: p. 70-82.
- 608 21. Bordage, M.-C., et al., *Implementation of new physics models for low energy*
609 *electrons in liquid water in Geant4-DNA*. Physica Medica, 2016. **32**(12): p. 1833-
610 1840.
- 611 22. Peudon, A., S. Edel, and M. Terrissol, *Molecular basic data calculation for radiation*
612 *transport in chromatin*. Radiation protection dosimetry, 2006. **122**(1-4): p. 128-135.
- 613 23. Salvat, F., A. Jablonski, and C.J. Powell, *ELSEPA—Dirac partial-wave calculation of*
614 *elastic scattering of electrons and positrons by atoms, positive ions and molecules*.
615 Computer Physics Communications, 2005. **165**(2): p. 157-190.
- 616 24. Frisch, M.J.T., G. W.; Schlegel, H. B.; Scuseria, G. E.; Robb, M. A.; Cheeseman, J.
617 R.; Scalmani, G.; Barone, V.; Mennucci, B.; Petersson, G. A.; Nakatsuji, H.; Caricato,
618 M.; Li, X.; Hratchian, H. P.; Izmaylov, A. F.; Bloino, J.; Zheng, G.; Sonnenberg, J.
619 L.; Hada, M.; Ehara, M.; Toyota, K.; Fukuda, R.; Hasegawa, J.; Ishida, M.; Nakajima,
620 T.; Honda, Y.; Kitao, O.; Nakai, H.; Vreven, T.; Montgomery, J. A., Jr.; Peralta, J. E.;
621 Ogliaro, F.; Bearpark, M.; Heyd, J. J.; Brothers, E.; Kudin, K. N.; Staroverov, V. N.;
622 Kobayashi, R.; Normand, J.; Raghavachari, K.; Rendell, A.; Burant, J. C.; Iyengar, S.
623 S.; Tomasi, J.; Cossi, M.; Rega, N.; Millam, J. M.; Klene, M.; Knox, J. E.; Cross, J.
624 B.; Bakken, V.; Adamo, C.; Jaramillo, J.; Gomperts, R.; Stratmann, R. E.; Yazyev,
625 O.; Austin, A. J.; Cammi, R.; Pomelli, C.; Ochterski, J. W.; Martin, R. L.; Morokuma,
626 K.; Zakrzewski, V. G.; Voth, G. A.; Salvador, P.; Dannenberg, J. J.; Dapprich, S.;
627 Daniels, A. D.; Farkas, Ö.; Foresman, J. B.; Ortiz, J. V.; Cioslowski, J.; Fox, D. J.,
628 *Gaussian 09, Revision D.01*. 2009: Wallingford, CT, USA.
- 629 25. Guerra, M., et al., *Single differential electron impact ionization cross sections in the*
630 *binary-encounter-Bethe approximation for the low binding energy regime*. Journal of
631 Physics B: Atomic, Molecular and Optical Physics, 2015. **48**(18): p. 185202.
- 632 26. Guest, M.F., et al., *The GAMESS-UK electronic structure package: algorithms,*
633 *developments and applications*. Molecular Physics, 2005. **103**(6-8): p. 719-747.
- 634 27. Mozejko, P. and L. Sanche, *Cross sections for electron scattering from selected*
635 *components of DNA and RNA*. Radiation Physics and Chemistry, 2005. **73**(2): p. 77-
636 84.
- 637 28. Huo, W.M., C.E. Dateo, and G.D. Fletcher, *Molecular data for a biochemical model*
638 *of DNA damage: Electron impact ionization and dissociative ionization cross sections*
639 *of DNA bases and sugar-phosphate backbone*. Radiation Measurements, 2006. **41**(9-
640 10): p. 1202-1208.
- 641 29. Vinodkumar, M., et al., *Electron impact total ionization cross sections for all the*
642 *components of DNA and RNA molecule*. International Journal of Mass Spectrometry,
643 2013. **339-340**: p. 16-23.
- 644 30. Akar, A. and H. Gümüş, *Electron stopping power in biological compounds for low*
645 *and intermediate energies with the generalized oscillator strength (GOS) model*.
646 Radiation Physics and Chemistry, 2005. **73**(4): p. 196-203.
- 647 31. Akar, A., H. Gümüş, and N. Okumuşoğlu, *Total electron stopping powers and CSDA-*
648 *ranges from 20 eV to 10 MeV electron energies for components of DNA and RNA*.
649 Advances in Quantum Chemistry, 2007. **52**: p. 277-288.
- 650 32. Akkerman, A. and E. Akkerman, *Characteristics of electron inelastic interactions in*
651 *organic compounds and water over the energy range 20–10000 eV*. Journal of
652 Applied Physics, 1999. **86**(10): p. 5809-5816.

- 653 33. Berger, M.J., et al. *ESTAR, PSTAR, and ASTAR: Computer Programs for Calculating*
654 *Stopping-Power and Range Tables for Electrons, Protons, and Helium Ions (version*
655 *1.2.3)*. 2005; Available from: <http://physics.nist.gov/Star>
- 656 34. Egan, E.P. and B.B. Luff, *Measurements at 15° to 80° C. - Density of Aqueous*
657 *Solutions of Phosphoric Acid*. Industrial & Engineering Chemistry, 1955. **47**(6): p.
658 1280-1281.
- 659 35. *ACD Labs Percepta Platform - PhysChem Module*. Available from:
660 <https://www.acdlabs.com/products/percepta/index.php>
- 661 36. Winstead, C. and V. McKoy, *Interaction of slow electrons with methyl phosphate*
662 *esters*. International Journal of Mass Spectrometry, 2008. **277**(1-3): p. 279-283.
- 663 37. Tonzani, S. and C.H. Greene, *Radiation damage to DNA: Electron scattering from the*
664 *backbone subunits*. The Journal of Chemical Physics, 2006. **125**(9): p. 094504.
- 665 38. Sakata, D., et al., *An implementation of discrete electron transport models for gold in*
666 *the Geant4 simulation toolkit*. Journal of Applied Physics, 2016. **120**(24): p. 244901.
- 667 39. Lampe, N., et al., *Mechanistic DNA damage simulations in Geant4-DNA part 1: A*
668 *parameter study in a simplified geometry*. Physica Medica, 2018. **48**: p. 135-145.
- 669 40. Lampe, N., *The long term impact of ionising radiation on living systems*. 2017, PhD
670 Thesis, Université Clermont Auvergne, France.
671